Effects of Cs Coverage and O/Te Incorporation Order on the Work Function of Cs/O/Te-activated GaAs(100)

Chaofeng Hu[1,2], Ziyi Ran[1,2], Tao Cui[1,2], Jie Yang[1,2], Meng Li[1], Xiaodong Yang[1] and Wei Liu[1,2,*]

[1]*Laboratory for Ultrafast Transient Facility, Chongqing University, Chongqing 400044, China*

[2]*College of Materials Science and Engineering, Chongqing University, Chongqing 400044, China*

Abstract: By lowering the vacuum energy level relative to the Fermi level, surface activation can reduce the work function of GaAs photocathodes, facilitating electron emission. Here, we use density functional theory to examine how Cs coverage and O/Te incorporation order affect the work function of Cs/O/Te-activated GaAs(100)-$\beta_2(2\times4)$. Cs-O-Te (O-first) and Cs-Te-O (Te-first) layers were compared over coverages of 1-11 Cs atoms per surface unit cell (0.14–1.57 monolayers on the nominal scale), with Cs-O as the conventional reference. At each Cs coverage, the ternary models had identical compositions but differed in their O/Te introduction sequences and associated initial site assignments. The total adsorption energy became more negative with increasing Cs coverage, whereas the average adsorption energy per Cs atom generally became less negative. All three systems exhibited nonmonotonic work-function changes with Cs coverage. Among the sampled configurations, the lowest work functions were 1.594 eV for 5Cs-O, 1.478 eV for 4Cs-O-Te, and 1.651 eV for 7Cs-Te-O. Cs-O-Te reached its discrete minimum at a lower Cs coverage than Cs-Te-O. Classical dipole-model fits captured the overall coverage dependence. Bader analysis showed that Cs atoms lost electrons on average, whereas O gained electrons, consistent with the charge-density-difference distributions. In Cs-O-Te, Te accumulated electrons at relatively low coverage; in Cs-Te-O, Te exhibited net electron depletion at lower coverage and net electron accumulation at higher coverage. The interfacial dipole varied with coverage in a manner qualitatively consistent with the work-function reduction. The work-function and adsorption-energy trends identify O-first activation at modest Cs loading as a promising starting point for dose optimization.

Keywords: GaAs photocathode; Cs/O/Te activation; Work function; Adsorption energy; Surface dipole.

1. INTRODUCTION

GaAs is a well-established III-V semiconductor photocathode material. For heavily p-type-doped GaAs, appropriate surface activation can lower the vacuum level and establish a negative electron affinity (NEA) state [1-3]. NEA GaAs photocathodes exhibit high quantum efficiency and low thermal emittance, making them attractive electron sources for accelerator and high-brightness applications [4-6]. Strained-layer and superlattice structures can further enhance electron spin polarization [7-9]. The emission properties of activated GaAs are strongly influenced by the atomic and electronic structure of the activation layer, in which adsorbate-induced charge redistribution and interfacial dipoles modify the vacuum-level alignment and electron-emission barrier [10-13].

Conventional Cs-O activation effectively lowers the GaAs surface work function and can yield high initial quantum efficiency. However, the resulting activation layer is chemically fragile and susceptible to residual-gas exposure, which can degrade the photoemission performance and limit the operational lifetime [14-17]. Te-containing activation schemes have been explored as an alternative strategy to improve the stability of activated GaAs photocathodes. Cs-Te and Cs-O-Te activation have been investigated experimentally [18, 19]. Recent studies have further indicated that Cs-Te activation can improve interfacial stability and operational lifetime while maintaining high quantum efficiency [20]. This motivates the present study of multicomponent Cs/O/Te activation layers.

Previous studies have shown that the electronic structure of activated GaAs depends on adsorption order [11, 21, 22]. For Cs/O/Te activation, the two incorporation orders may produce different interfacial configurations, with corresponding differences in charge redistribution, dipole formation, and work function. Comparing Cs-O-Te (O-first) and Cs-Te-O (Te-first) under a common site-selection rule provides a way to examine these differences at identical stoichiometry.

*Address correspondence to this author at Laboratory for Ultrafast Transient Facility, Chongqing University, Chongqing 400044, China;
E-mail: weiliu@cqu.edu.cn

Received on 02-09-2026 Accepted on 31-10-2026 Published on 11-11-2026

E-ISSN: 3110-9772/26

We use density functional theory (DFT) to compare Cs-O-Te and Cs-Te-O activation layers on GaAs(100)-$\beta_2(2\times4)$ over 1–11 Cs atoms per cell, with Cs-O as the reference. The relaxed structures, adsorption energies, work functions, and charge redistribution are examined to relate the coverage response to the O/Te configurations.

2. COMPUTATIONAL METHODS AND MODELS

2.1. Computational Details

Density functional theory (DFT) calculations were performed using the Vienna Ab initio Simulation Package (VASP) [23, 24]. The interaction between valence electrons and ionic cores was described using the projector augmented-wave (PAW) method [25], and exchange-correlation effects were treated using the Perdew-Burke-Ernzerhof (PBE) functional within the generalized gradient approximation (GGA) [26]. The adsorption systems were treated using non-spin-polarized calculations, whereas spin polarization was included in the isolated-atom reference calculations for adsorption energies. The valence-electron configurations included in the PAW potentials were $\mathrm{Ga}: 3d^{10}4s^24p^1$; $\mathrm{As}: 4s^24p^3$; $\mathrm{Zn}: 3d^{10}4s^2$; $\mathrm{Cs}: 5s^25p^66s^1$; $O: 2s^22p^4$; and $\mathrm{Te}: 5s^25p^4$.

A plane-wave cutoff energy of 510 eV was adopted based on the cutoff energies of the employed PAW potentials. With reference to previous first-principles studies of GaAs(100)-$\beta_2(2\times4)$ [22, 27], the electronic self-consistency criterion was set to 1.0 × 10^{-6} eV. Structural relaxation continued until the residual force on each unconstrained atom was below 0.01 eVÅ^{-1}. A dipole correction was applied along the surface-normal (z) direction to reduce spurious electrostatic interactions between periodically repeated asymmetric slabs [28]. With the lattice parameters fixed, structures were first relaxed using a 1 × 1 × 1 k-point mesh and then further relaxed using a 6 × 3 × 1 Monkhorst-Pack mesh [29]. Final self-consistent single-point calculations used the 6 × 3 × 1 mesh and Gaussian smearing with a width of 0.05 eV to obtain the total energies, Fermi levels, electrostatic potentials, and charge densities.

2.2. Surface Model and Construction

In our previous study, in situ microspot low-energy electron diffraction (μLEED) measurements after thermal cleaning of GaAs at 610 °C revealed a (2 × 4) surface periodicity [20]. Guided by this observation and established structural studies [30, 31], we adopted the As-rich GaAs(100)-$\beta_2(2\times4)$ reconstruction as the reference surface model. The PBE-optimized bulk lattice constant of GaAs was 5.75 Å, close to the experimental value of approximately 5.65 Å. The resulting Zn-doped surface slab had lattice parameters of a = 8.134 Å, b = 16.268 Å, and c = 30.065 Å, as illustrated in Fig. (**1**). The adsorbate-free slab was constructed with a vacuum region of approximately 19.7 Å along the surface normal to accommodate the outward extension of the adsorption layer at higher Cs coverages and reduce interactions between periodically repeated slabs. The model contained 28 As atoms, 21 Ga atoms, one substitutional Zn atom, and eight H atoms used to passivate the dangling bonds at the bottom surface. As the experimental photocathode activation was performed on heavily Zn-doped p-type GaAs, one Ga atom in the slab was substituted with Zn to represent the acceptor doping, corresponding to 4.55% of the Ga-sublattice sites. During structural relaxation, the bottom three substrate atomic planes, including the Zn atom, and the H atoms were kept fixed, while the remaining substrate atoms and all adsorbates were allowed to relax.

The optimized GaAs(100)-$\beta_2(2\times4)$ surface, shown in Fig. (**1**), exhibits two As–As dimers in the topmost layer and one in the third layer, with bond lengths of 2.490 Å for each top-layer dimer and 2.582 Å for the third-layer dimer, consistent with the experimentally reported value of 2.48$\pm$0.20 Å obtained from reflection high-energy electron diffraction measurements [31]. The calculated work function of the adsorbate-free GaAs surface was 4.987 eV, providing a reference for evaluating activation-induced work-function changes.

Cs-O, Cs-O-Te, and Cs-Te-O models containing 1–11 Cs atoms per cell were constructed from the same Cs-precovered GaAs structures, using the Cs site hierarchy established in our previous study [20]. At each coverage, the ternary models contained identical Cs populations, one O atom, and one Te atom. Keeping the O and Te populations fixed allows the two ternary configurations to be compared at matched composition at each Cs coverage. In that study, adding an eighth Cs atom produced a relaxed configuration with one Cs atom appreciably farther from the substrate. Following that structural reference, seven Cs atoms per cell define a nominal monolayer (ML), which also provides the coverage scale for the classical dipole-model fits. One nominal ML corresponds to approximately 5.29 × 10^{14} atoms/cm^2, and 1–11 Cs spans 0.14–1.57 ML. This range includes the sampled work-function minima and the subsequent increase at

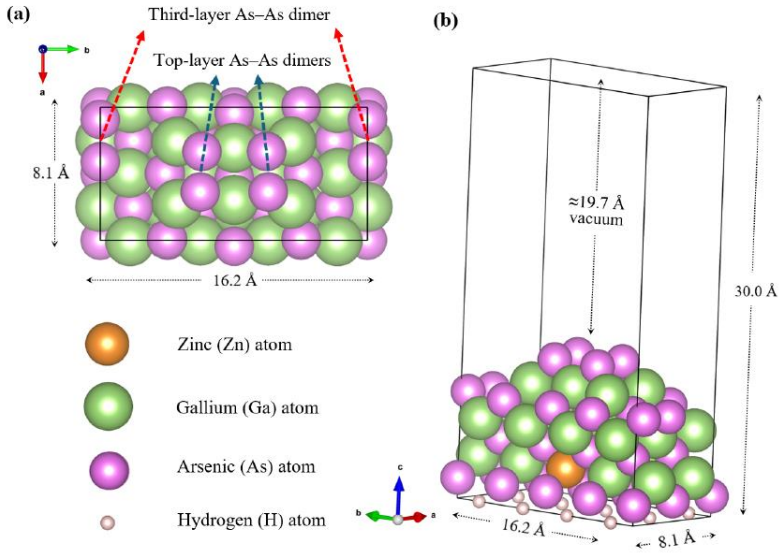


Figure 1: Top and side views of the optimized, adsorbate-free GaAs(100)-β_2(2 × 4) surface model. (a) Top view showing two As–As dimers in the outermost layer and one As–As dimer in the third layer. (b) Side view of the periodically repeated slab, including the substitutional Zn dopant, H-passivated bottom surface, and vacuum region. The solid lines indicate the simulation cell.

higher coverage. This model-specific nominal scale provides a common coverage normalization for the three adsorption systems.

The two ternary systems were constructed using different O/Te introduction orders under a common site-selection rule motivated by experimental surface activation. Matching the Cs-precovered starting structures, composition, and relaxation settings provides a controlled comparison of the relaxed configurations generated by the two construction sequences. The Cs adsorption-site ranking established previously served as a common geometric reference for placing O and Te. Relaxation after the first introduction step established the local environment encountered by the second species. For Cs-O-Te, O was first placed at the highest-ranked Cs adsorption site, and the Cs atom initially occupying that site was displaced by 3–4 Å toward the vacuum. This first placement and relaxation step also generated the Cs-O reference configuration. After relaxation, Te was placed at the next-ranked Cs adsorption site. Any Cs atom occupying that site was displaced in the same manner before the second relaxation. Cs-Te-O was constructed in the reverse order, with Te introduced first, followed by O. For the 1Cs configuration in either system, the single Cs atom was displaced only when the first species was introduced. The second site was vacant, so the second species was placed there without further Cs displacement, followed by structural relaxation. Both introduction stages used the atomic constraints and force criterion specified above. The comparison includes the O/Te introduction sequence and its associated initial site assignments within the same GaAs(100)-β_2(2 × 4) cell.

3. RESULTS AND DISCUSSION

3.1. Structural Evolution

Fig. (**2**) compares representative relaxed Cs-O-Te and Cs-Te-O configurations at 4 Cs and 10 Cs per cell. These configurations represent relatively low and high Cs coverages, respectively. At each coverage, the ternary models have identical stoichiometry and were generated using different O/Te incorporation orders under the common site-selection rule.

As shown in Fig. (**2**), local rearrangements of surface As and Ga atoms near the adsorbates occur at both low and high Cs coverages for both ternary systems. After relaxation, Cs atoms lie mainly above the GaAs surface, while O and Te occupy localized adsorption regions near the surface. Their arrangements relative to neighboring Cs and substrate atoms nevertheless differ between the two systems. Such differences in local coordination can modify interfacial charge redistribution and surface-normal polarization, affecting the electronic response discussed below.

At higher Cs coverages, Cs accumulation toward the outer region of the adsorbate layer becomes

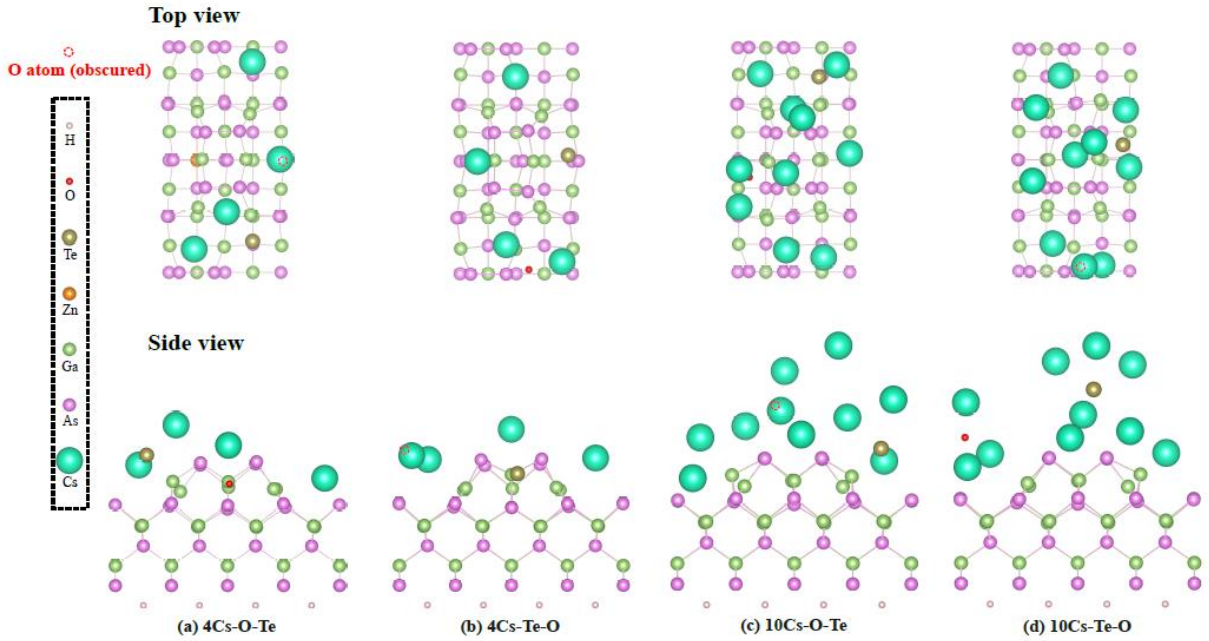


Figure 2: Relaxed structures of the Cs-O-Te and Cs-Te-O ternary activation systems at different Cs coverages: (a) 4Cs-O-Te, (b) 4Cs-Te-O, (c) 10Cs-O-Te, and (d) 10Cs-Te-O. The 4 Cs and 10 Cs configurations represent relatively low and high Cs coverages, respectively. Top and side views are shown for each configuration. The red dashed circle marks the position of an O atom obscured by neighboring atoms in the corresponding viewing direction.

increasingly pronounced following structural relaxation. Compared with the low-coverage configurations, the O atom introduced first in Cs-O-Te and the Te atom introduced first in Cs-Te-O lie closer to the outer region of the adsorbate layer and are more highly coordinated with surrounding Cs atoms. The subsequently introduced species remain close to the substrate: Te lies between the GaAs surface and the outer Cs layer in 10Cs-O-Te, while O occupies a near-surface adsorption region in 10Cs-Te-O. At higher Cs coverage, adsorbate-layer rearrangements may enhance depolarization and reduce the effective dipole contribution per Cs atom. This provides a possible explanation for the work-function increase beyond the minimum.

3.2. Coverage Dependence of Adsorption Energy

The total adsorption energy, E_{ads}, and the average adsorption energy per Cs atom, $E_{\mathrm{ads}}^{\mathrm{Cs}}$, were calculated to assess the coverage dependence of adsorption in the Cs-O, Cs-O-Te, and Cs-Te-O systems. E_{ads} describes the total energy change associated with the formation of the adsorbate layer relative to the clean GaAs surface and isolated-atom references, whereas $E_{\mathrm{ads}}^{\mathrm{Cs}}$ describes the average energy change per Cs atom upon adsorption relative to the corresponding non-Cs reference surface and isolated Cs atoms. These adsorption energies were calculated as follows:

$$E_{\mathrm{ads}} = \begin{cases} E_{\mathrm{GaAs+Cs-O}} - E_{\mathrm{GaAs}} - nE_{\mathrm{Cs}} - E_{\mathrm{O}}, \\ E_{\mathrm{GaAs+Cs-O-Te/Cs-Te-O}} - E_{\mathrm{GaAs}} - nE_{\mathrm{Cs}} - E_{\mathrm{O}} - E_{\mathrm{Te}}. \end{cases} \quad (1)$$

$$E_{\mathrm{ads}}^{\mathrm{Cs}} = \begin{cases} \frac{1}{n}(E_{\mathrm{GaAs+Cs-O}} - E_{\mathrm{GaAs-O}} - nE_{\mathrm{Cs}}), \\ \frac{1}{n}(E_{\mathrm{GaAs+Cs-O-Te}} - E_{\mathrm{GaAs+O+Te}} - nE_{\mathrm{Cs}}), \\ \frac{1}{n}(E_{\mathrm{GaAs+Cs-Te-O}} - E_{\mathrm{GaAs+O+Te}} - nE_{\mathrm{Cs}}). \end{cases} \quad (2)$$

Here, $E_{\mathrm{GaAs+Cs-O}}$, $E_{\mathrm{GaAs+Cs-O-Te}}$, and $E_{\mathrm{GaAs+Cs-Te-O}}$ represent the total energies of the corresponding adsorption systems, and E_{GaAs} is the total energy of the clean GaAs surface. E_{Cs}, E_{O}, and E_{Te} are the energies of isolated Cs, O, and Te atoms, respectively, and n denotes the number of adsorbed Cs atoms. $E_{\mathrm{GaAs-O}}$ is the total energy of the Cs-free O/GaAs reference used for the Cs-O series. Both ternary series use the same Cs-free reference energy, $E_{\mathrm{GaAs+O+Te}}$, corresponding to the relaxed GaAs surface containing one O and one Te atom. This reference was obtained by initially placing both adsorbates above the surface and relaxing the atomic positions. The reference was relaxed using the computational settings, atomic constraints, and convergence criteria described in Section 2. Its energy is independent of n and was used at every Cs coverage in both ternary series. More negative values indicate a more favorable adsorption process under the corresponding reference definition.

As shown in Fig. (**3a**), the total adsorption energies of all three systems become progressively more

negative as the Cs coverage increases from 1 Cs to 11 Cs per cell. This behavior mainly originates from the increasing number of adsorbed Cs atoms and the structural relaxation of the adsorption layer. The total adsorption energies of Cs-O-Te and Cs-Te-O can be compared directly because the systems have identical compositions at each coverage. Cs-O-Te has a more negative total adsorption energy than Cs-Te-O at low coverage, but the difference decreases with increasing Cs coverage and becomes small at high coverage.

The ternary systems contain an additional Te atom relative to Cs-O, so their total adsorption energies include an additional adsorbate contribution. Coverage dependent trends are therefore examined within each series, while direct comparisons between the two O/Te incorporation sequences use the composition-matched ternary structures.

Fig. (**3b**) compares the average Cs adsorption energies relative to the specified Cs-free reference surfaces. At low Cs coverage, Cs-O-Te has a more negative $E_{\mathrm{ads}}^{\mathrm{Cs}}$ than Cs-Te-O when evaluated against their common relaxed O/Te-containing reference. As Cs coverage increases, $E_{\mathrm{ads}}^{\mathrm{Cs}}$ generally becomes less negative for all three systems, indicating that Cs adsorption becomes less favorable on average. This trend may be associated with stronger Cs-Cs interactions and rearrangement of the adsorbate layer as coverage increases.

Across a broad coverage range, both Te-containing systems have more negative $E_{\mathrm{ads}}^{\mathrm{Cs}}$ values than Cs-O when evaluated against their respective non-Cs reference systems. The average Cs adsorption energies of the two ternary systems gradually converge at high coverage.

3.3. Work Function and Charge Redistribution

The work function is the energy required to transfer an electron from the Fermi level to vacuum. Adsorption-induced charge redistribution and interfacial dipoles can shift the vacuum level and modify the work function. The electron affinity, $\chi = E_{\mathrm{vac}} - E_{\mathrm{CBM}}$, is instead referenced to the conduction-band minimum E_{CBM}, with NEA corresponding to $\chi < 0$. The work function is calculated as

$$\Phi = E_{\mathrm{vac}} - E_F, \tag{3}$$

where E_{vac} is the vacuum level extracted from the plateau of the planar-averaged electrostatic potential on the activated surface side of the slab, and E_{F} is the Fermi level obtained from the same final self-consistent calculation. Representative planar-averaged electrostatic potential profiles for the 1Cs–O–Te, 6Cs–O–Te, and 11Cs–O–Te configurations are presented in Supplementary Fig. S1, confirming the presence of identifiable vacuum plateaus on the activated side across representative Cs coverages.

Figure (**4**) shows a nonmonotonic coverage dependence for all three systems: the work function decreases, reaches a minimum, and then increases. The lowest sampled values are 1.594 eV for 5Cs-O, 1.478 eV for 4Cs-O-Te, and 1.651 eV for 7Cs-Te-O. Thus, the 4Cs- O-Te minimum is 0.116 eV below the 5Cs-O minimum, which occurs at a different coverage.

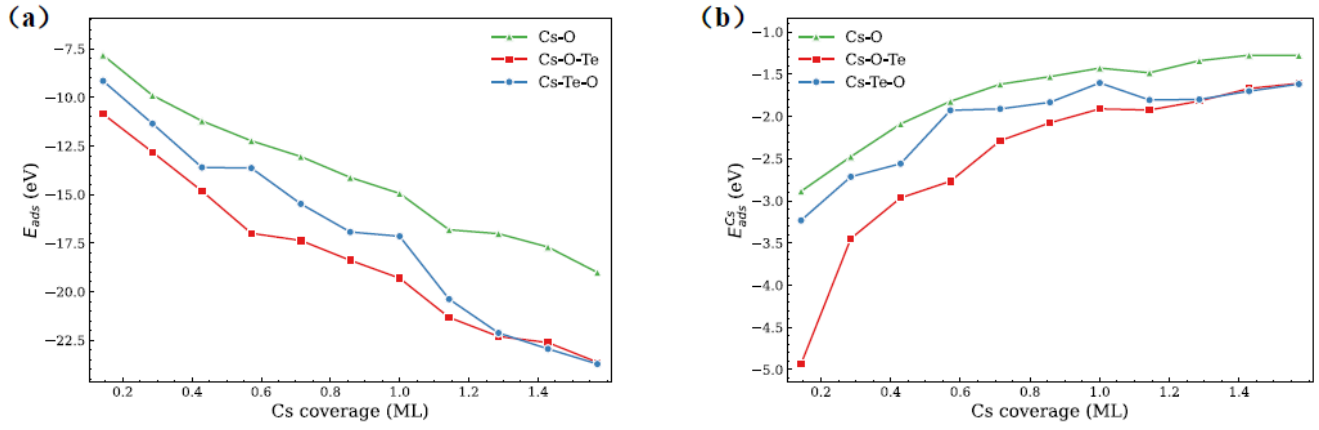


Figure 3: Adsorption energies as functions of Cs coverage for Cs-O, Cs-O-Te, and Cs-Te-O: (a) total adsorption energy, E_{ads}; (b) average Cs adsorption energy, $E_{\mathrm{ads}}^{\mathrm{Cs}}$. Cs-O is included as the conventional reference. Cs coverage follows the definition in Section 2.2, with 7 Cs corresponding to 1 ML.

Their relative ordering is retained in the representative electronic-setting and spin-polarization checks reported in the Supplementary Information.

The two ternary systems exhibit different work-function responses despite their identical compositions at each Cs coverage. Cs-Te-O generally has a higher work function than Cs-O at low coverage, showing that Te incorporation does not uniformly lower the work function. Within each ternary series, Cs coverage varies at fixed O and Te populations, so the Cs:O:Te ratio changes. The observed responses describe the accompanying changes in local structure and charge redistribution under these fixed O and Te loadings.

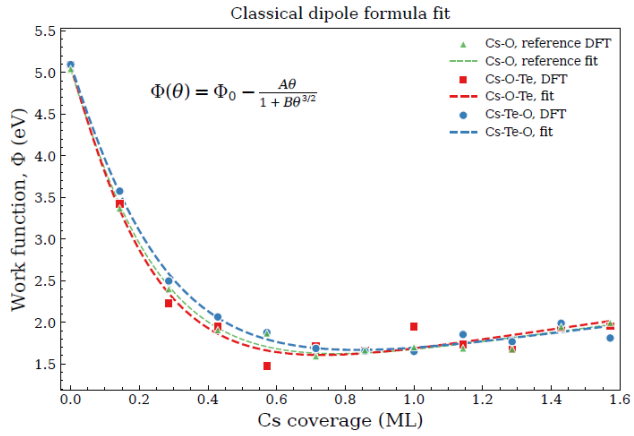


Figure 4: Coverage-dependent work functions of the Cs-O, Cs-O-Te, and Cs-Te-O systems. Symbols represent the work functions of the sampled DFT configurations, whereas dashed curves describe their overall coverage dependence using the classical dipole model, $\Phi(\theta) = \Phi 0 - A\theta/(1 + B\theta^{3/2})$ [32]. Cs-O is included as the conventional reference, and the ML scale follows the coverage definition in Section 2.2.

The classical coverage-dependent dipole model was fitted to the discrete DFT values to summarize the overall trend. The fitted expression is

$$\Phi(\theta) = \Phi_0 - \frac{A\theta}{1+B\theta^{3/2}}, \quad (4)$$

where the Cs coverage is defined as

$$\theta = \frac{N_{Cs}}{7}, \quad (5)$$

with NCs denoting the number of Cs atoms per surface unit cell and 7 Cs corresponding to 1 ML, as defined in Section 2.2. Here, Φ_0 is fixed at the work function of the corresponding Cs-free reference surface, retaining one O atom for Cs-O (5.0411 eV) and one O plus one Te atom for both ternary systems (5.0931 eV). The parameter A controls the initial slope of the work-function decrease, and B phenomenologically accounts for dipole-dipole interactions and depolarization as coverage increases. The fitted parameters and root-mean-square errors (RMSEs) for the 1–11 Cs data are given in Supplementary Table S2.

Table **1** summarizes the continuous fitted minima alongside the lowest sampled DFT values. The fitted minima of Cs-O and Cs-O-Te are comparable, whereas Cs-Te-O has a higher fitted minimum. The fits describe the overall coverage dependence; the discrete DFT values identify the lowest-work-function configurations calculated explicitly. The charge analysis below examines the electronic redistribution associated with these coverage responses.

Table 1: Work-function Minima from the Classical Dipole-model Fits and the Sampled Discrete DFT Configurations. Fitted Minima Characterize the Empirical Curves, Whereas DFT Minima Identify the Lowest Calculated Values Within the Configurations Examined. Coverage is Defined as $\theta = N_{Cs}/7$.

System	θ_{min}^{fit} (ML)	Φ_{min}^{fit} (eV)	θ_{min}^{DFT} (ML)	Φ_{min}^{DFT} (eV)
Cs-O	0.78	1.624	0.71	1.594
Cs-O-Te	0.73	1.608	0.57	1.478
Cs-Te-O	0.83	1.669	1.00	1.651

To quantify charge redistribution involving the adsorbates, net Bader charge analysis was performed using the zero-flux partitioning algorithm [33]. The net charge of atom i is defined as

$$\Delta q_i = N_i^{val} - N_i^{Bader}, \quad (6)$$

where N_i^{val} is the valence-electron count of neutral atom i and N_i^{Bader} is the number of electrons in its Bader basin. Positive and negative values of Δq_i denote net electron depletion and accumulation, respectively. Bader net charges are distinct from formal oxidation states.

Figure (**5a**) illustrates interfacial charge redistribution in the two ternary systems, and Fig. (**5b,c**) presents the adsorbate Bader net charges as functions of Cs coverage. The Cs values are averaged over all Cs atoms at each coverage. This average remains positive throughout the investigated range, whereas the net charge of O remains negative, indicating electron loss from Cs on average and electron gain by O. The net charge of Te varies with both the O/Te incorporation order and Cs coverage.

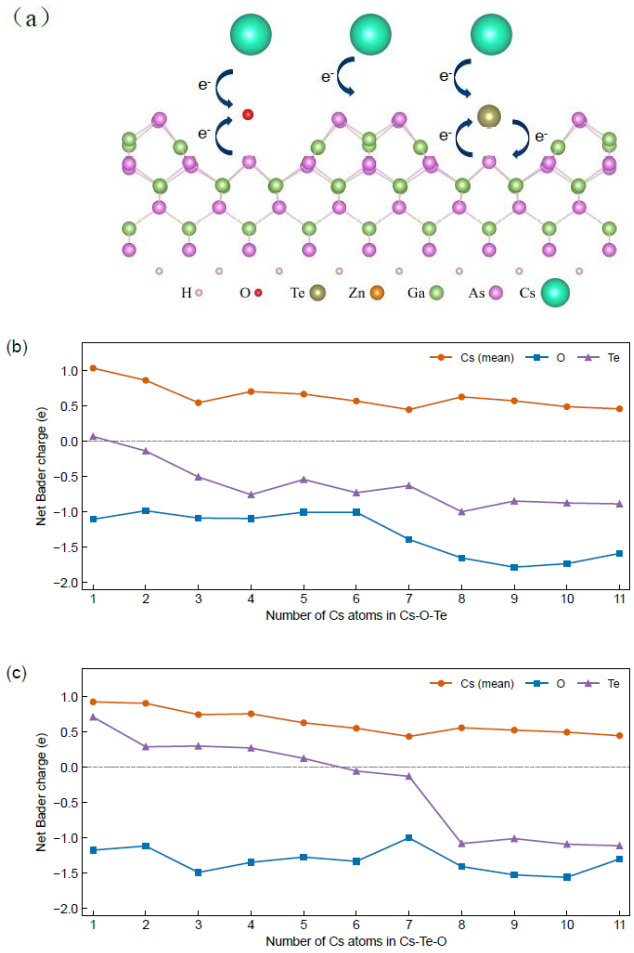


Figure 5: Interfacial charge redistribution and coverage-dependent Bader net charges in Cs-O-Te and Cs-Te-O. (a) Schematic illustration of interfacial charge redistribution. (b,c) Bader net charges of Cs, O, and Te in Cs-O-Te and Cs-Te-O, respectively. The Cs values are averaged over all Cs atoms at each coverage, whereas the O and Te values each correspond to one atom per surface cell. Positive and negative values denote net electron depletion and accumulation, respectively.

To complement the Bader analysis, the spatial pattern of electron redistribution was examined using the charge-density difference (CDD), defined as

$$\Delta\rho(\boldsymbol{r}) = \rho_{\mathrm{tot}}(\boldsymbol{r}) - \rho_{\mathrm{GaAs}}(\boldsymbol{r}) - \sum_{\alpha}\rho_{\alpha}(\boldsymbol{r}), \quad (7)$$

where ρ_{tot} (r), ρ_{GaAs}(r), and ρ_{α}(r) are the electron densities of the complete adsorption system, the GaAs slab, and the separated adsorbate component α, respectively. All reference densities were calculated in the same simulation cell, with the constituent atoms fixed at their positions in the complete system. Positive and negative values of $\Delta\rho$ denote electron accumulation and depletion, respectively.

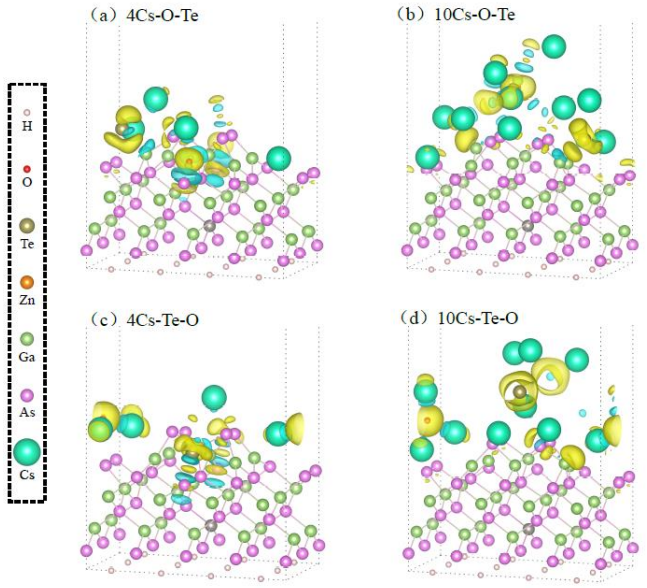


Figure 6: Charge-density-difference isosurfaces for Cs-O-Te and Cs-Te-O at 4 Cs and 10 Cs coverages: (a) 4Cs-O-Te, (b) 10Cs-O-Te, (c) 4Cs-Te-O, and (d) 10Cs-Te-O. Yellow and cyan indicate electron accumulation and depletion, respectively. Iso-surface values of $\pm$0.0035 e/Å^3 are used for all configurations.

The CDD isosurfaces in Fig. (**6**) show electron accumulation around O in both ternary systems at 4 Cs and 10 Cs, consistent with its negative net Bader charge. In 4Cs-O-Te, electron accumulation is also visible around Te, accompanied by depletion around neighboring Cs atoms on the vacuum side and in parts of the substrate. In 4Cs-Te-O, accumulation and depletion regions coexist around Te, but its positive net Bader charge indicates net electron loss within the Te basin. The relaxed configurations obtained with the two O/Te incorporation orders therefore exhibit different local polarization around Te.

In 10Cs-O-Te, electron accumulation persists around Te, consistent with its net Bader charge remaining negative. For Cs-Te-O, Te has a net Bader charge of approximately +0.13e at 5 Cs, is close to neutral at 6 Cs (−0.05e), and exhibits negative net charges at 7–11 Cs. This coverage dependence indicates net electron depletion at lower coverage and net electron accumulation at higher coverage. The corresponding CDD isosurfaces at 5–8 Cs are shown in Supplementary Fig. S4. Consistent with this change, the CDD of 10Cs-Te-O exhibits electron accumulation around Te, while neighboring Cs atoms predominantly show electron depletion. These contrasting charge distributions characterize the local environments obtained with the two construction sequences.

To quantify the associated interfacial charge separation, the CDD was integrated over the VASP fast Fourier transform (FFT) grid. The electron-number change associated with grid point i is denoted by δq_i, and the effective redistributed charge is defined as

$$Q = \frac{1}{2}\left(\sum_{\delta q_i>0} \delta q_i - \sum_{\delta q_i<0} \delta q_i\right), \quad (8)$$

where positive and negative values of δqi denote electron accumulation and depletion, respectively. Thus, Q is the mean of the total accumulated electron number and the magnitude of the total depleted electron number.

The signed separation between the electron-depletion and electron-accumulation centers along the surface normal is defined as

$$d_z = \frac{\sum_i \delta q_i z_i}{\sum_i \delta q_i}|_{\delta q_i<0} - \frac{\sum_i \delta q_i z_i}{\sum_i \delta q_i}|_{\delta q_i>0}. \quad (9)$$

where z_i is the surface-normal coordinate of grid point i, with the positive direction pointing from the GaAs slab toward the vacuum. The periodic grid was referenced to a common vacuum cut at $z_{\mathrm{cut}} = 26.5$ Å, where the CDD is small and the calculated dipoles are insensitive to nearby cuts. The coordinates were mapped as $z_i = (z_i^{\mathrm{cell}} - z_{\mathrm{cut}})\, mod\, L_z$, with L_z denoting the cell length along the surface normal. Thus, $d_z > 0$ indicates that the electron-depletion center lies farther toward the vacuum than the electron-accumulation center.

The surface-normal interfacial dipole moment is calculated as

$$\mu_\perp = Q d_z, \quad (10)$$

where Q is expressed in units of e and d_z in Å, giving $\mu_\perp$ in $eÅ$.

As shown in Fig. (**7**), the interfacial dipole moment increases at low Cs coverage and varies more gradually at higher coverage. A relatively large dipole develops at lower coverage in Cs-O-Te than in Cs-Te-O. The work-function reduction is defined as $\Delta\Phi = \Phi_{\mathrm{GaAs}} - \Phi$, where $\Phi_{\mathrm{GaAs}} = 4.987$ eV is the work function of the adsorbate-free GaAs surface. For a surface dipole layer, the dipole-induced vacuum-level shift scales with the surface-normal dipole moment per unit area. Across the 11 calculated coverages, linear fits of $\Delta\Phi$ against $\mu_\perp$ give $R^2 = 0.979$ for Cs-O-Te and $R^2 = 0.971$ for Cs-Te-O, supporting a strong positive association within each series. The fitted parameters and residuals are reported in the Supplementary Information. The work-function reduction contains both a vacuum-level contribution and a Fermi-level contribution, $\Delta\Phi = (E_{\mathrm{vac}}^0 - E_{\mathrm{vac}}) + (E_{\mathrm{F}} - E_{\mathrm{F}}^0)$, where the superscript 0 denotes the adsorbate-free reference. Structural rearrangements change local coordination and charge redistribution, while Fermi-level shifts provide an additional contribution to the work-function change. These effects can contribute to deviations from a simple proportional relation between the CDD-derived dipole and $\Delta\Phi$.

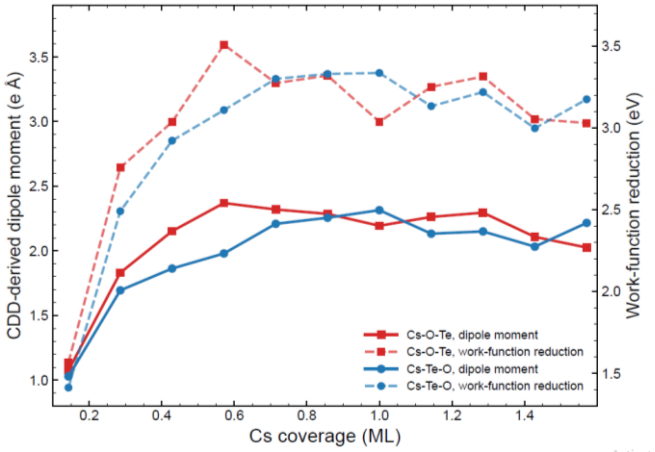


Figure 7: The interfacial dipole moment, $\mu_\perp$, and work function reduction as functions of Cs coverage for Cs-O-Te and Cs-Te-O. Solid lines denote $\mu_\perp$ (left axis), and dashed lines denote the work-function reduction (right axis). Cs coverage follows the definition in Section 2.2, with 7 Cs corresponding to 1 ML.

The total adsorption energy becomes more negative as Cs coverage increases, whereas the work function passes through a minimum. The coverage response is therefore not captured by adsorption energetics alone. The charge and dipole analyses instead relate the work function trend to changes in interfacial charge separation.

4. CONCLUSION

In this work, first-principles calculations were performed to compare Cs-O-Te and Cs-Te-O activation layers on GaAs(100)-$\beta_2(2\times4)$, using Cs-O as the conventional reference. Cs coverages from 1 to 11 atoms per surface unit cell were considered. At each Cs coverage, the ternary models have identical stoichiometry and were constructed using a common site-selection rule. The comparison includes the different initial O/Te site assignments associated with the two incorporation orders.

The total adsorption energy becomes more negative with increasing Cs coverage for all systems, reflecting

the cumulative energy gain associated with adsorbate-layer formation. In contrast, the average Cs adsorption energy generally becomes less negative, indicating weaker average energetic stabilization per Cs atom at higher coverage. This weakening raises the possibility that Cs-rich layers may be more susceptible to rearrangement or desorption under laser-induced heating.

The work functions of all three systems exhibit a nonmonotonic dependence on Cs coverage. Among the sampled configurations, 4Cs-O-Te yields the lowest calculated work function of 1.478 eV, compared with 1.594 eV for 5Cs-O and 1.651 eV for 7Cs-Te-O. The different discrete minimum positions indicate that the O/Te configurations affect the Cs coverage range favorable for work-function reduction. Classical dipole-model fits summarize the overall coverage dependence. The lower Cs coverage required by Cs-O-Te in this comparison motivates experimental tests of whether O-first activation can reduce the Cs dose needed to reach a low-work function state.

The net Bader charge and charge-density-difference analyses show net electron depletion from Cs on average and electron accumulation on O. The net charge of Te is more sensitive to both the O/Te introduction order and Cs coverage. In Cs-O-Te, Te exhibits net electron accumulation at relatively low coverage. In Cs-Te-O, Te is close to neutral at 6 Cs and exhibits net electron accumulation at 7–11 Cs. The interfacial dipole follows a similar coverage dependence and is qualitatively consistent with the shift of the coverage range for low work function, although the two quantities do not have a strict one-to-one correspondence.

Within the sampled configurations, Cs-O-Te reaches a lower work-function minimum at lower Cs coverage, where average Cs adsorption is more favorable. At the fixed O and Te loadings examined here, these results provide a basis for jointly considering Cs loading and O/Te introduction order in activation optimization. Experiments varying the relative Cs, O, and Te doses under controlled illumination and residual-gas exposure could assess the implications for quantum efficiency and operational stability.

FUNDING

This work was supported by the National Natural Science Foundation of China (Grant No. 12405180) and the Fundamental Research Funds for the Central Universities, China (Grant No. 2024CDJXY004)

DATA AVAILABILITY

The atomic structures, representative VASP input settings and numerical adsorption-energy, work-function, Bader-charge, and dipole data are provided in the accompanying Supplementary_Data package.

CONFLICT OF INTEREST

The authors declare no conflict of interest.

REFERENCES

[1] Spicer WE. Negative Affinity 3–5 Photocathodes: Their Physics and Technology. *Appl. Phys.* 1977; 12:115–30

[2] Stocker BJ. AES and LEED Study of the Activation of GaAs–Cs–O Negative Electron Affinity Surfaces. *Surf. Sci.* 1975; 47:501–13

[3] Hu C, Ran Z, Cui T, *et al.* Research progress of GaAs-based spin-polarized photocathodes and their applications. *Acta Physica Sinica* 2026; 75:(accepted)

[4] Wang X, Shi M, Su L, *et al.* NEA GaAs Photocathode for Electron Source: From Growth, Cleaning, Activation to Performance. *Mater. Today Phys.* 2025; 52:101680

[5] Bazarov IV, Dunham BM, Li Y, *et al.* Thermal Emittance and Response Time Measurements of Negative Electron Affinity Photocathodes. *J. Appl. Phys.* 2008; 103:054901

[6] Xiang R and Teichert J. Photocathodes for High Brightness Photo Injectors. *Phys. Procedia* 2015; 77:58–65

[7] Pierce DT, Meier F, and Zürcher P. Negative Electron Affinity GaAs: A New Source of Spin-Polarized Electrons. *Appl. Phys. Lett.* 1975; 26:670–2

[8] Maruyama T, Luh DA, Brachmann A, *et al.* Systematic Study of Polarized Electron Emission from Strained GaAs/GaAsP Superlattice Photocathodes. *Appl. Phys. Lett.* 2004; 85:2640–2

[9] Liu W, Chen Y, Lu W, *et al.* Record-level quantum efficiency from a high polarization strained GaAs/GaAsP superlattice photocathode with distributed Bragg reflector. *Applied Physics Letters* 2016; 109(25):252104

[10] Su CY, Spicer WE, and Lindau I. Photoelectron Spectroscopic Determination of the Structure of (Cs,O) Activated GaAs (110) Surfaces. *J. Appl. Phys.* 1983; 54:1413–22

[11] Sada Y and Meguro T. Study on Work Function and Corresponding Electron Emission during NEA Activation of GaAs Surfaces. *Appl. Surf. Sci.* 2020; 513:145699

[12] Zhang K, Zhang J, Zhang Y, *et al.* Exploration of Cs–O Co-Adsorption on GaAs(100) β2(2 × 4) Surface at Different Sites from First-Principles Calculation. *Mater. Sci. Semicond. Process.* 2021; 134:105996

[13] Li S, Zhang Y, Zhang K, *et al.* Comparison of Activation Behavior of Cs–O and Cs–NF3-Adsorbed GaAs(100)-β2(2 × 4) Surface: From DFT Simulation to Experiment. *J. Colloid Interface Sci.* 2022; 613:117–25

[14] Chanlek N, Herbert JD, Jones RM, *et al.* The Degradation of Quantum Efficiency in Negative Electron Affinity GaAs Photocathodes under Gas Exposure. *J. Phys. D: Appl. Phys.* 2014; 47:055110

[15] Wada T, Nitta T, Nomura T, *et al.* Influence of Exposure to CO, CO2 and H2O on the Stability of GaAs Photocathodes. *Jpn. J. Appl. Phys.* 1990; 29:2087–91

[16] Durek D, Frommberger F, Reichelt T, *et al.* Degradation of a Gallium-Arsenide Photoemitting NEA Surface by Water Vapour. *Appl. Surf. Sci.* 1999; 143:319–22

[17] Pastuszka S, Terekhov AS, and Wolf A. Stable to Unstable Transition in the (Cs,O) Activation Layer on GaAs(100)

Surfaces with Negative Electron Affinity in Extremely High Vacuum. *Appl. Surf. Sci.* 1996; 99:361–5

[18] Biswas J, Wang E, Gaowei M, *et al.* High Quantum Efficiency GaAs Photocathodes Activated with Cs, O2, and Te. *AIP Adv.* 2021; 11:025321

[19] Bae JK, Andorf MB, Bazarov IV, *et al.* Optimizing Activation Recipe with Cs, Te, O for GaAs-Based Photocathodes. *Proc. 13th Int. Particle Accelerator Conf. (IPAC'22)*. Bangkok, Thailand, 2022 :628–30

[20] Liu W, Hu C, Ran Z, *et al.* Engineering Stable Interfaces: Cs–Te Activation for Long-Lifetime GaAs Photocathodes. *Appl. Surf. Sci.* 2026; 728:166069

[21] Kamaratos M. Adsorption Kinetics of the Cs–O Activation Layer on GaAs(100). *Appl. Surf. Sci.* 2001; 185:66–71

[22] Zhang J, Zhang Y, Qian Y, *et al.* First-Principles Investigation of Cs–NF3 Co-Adsorption on GaAs(100)-β2(2×4) Surface. *Appl. Surf. Sci.* 2021; 535:147691

[23] Kresse G and Furthmüller J. Efficiency of Ab-Initio Total Energy Calculations for Metals and Semiconductors Using a Plane-Wave Basis Set. *Comput. Mater. Sci.* 1996; 6:15–50

[24] Kresse G and Furthmüller J. Efficient Iterative Schemes for Ab Initio Total-Energy Calculations Using a Plane-Wave Basis Set. *Phys. Rev. B* 1996; 54:11169–86

[25] Kresse G and Joubert D. From Ultrasoft Pseudopotentials to the Projector Augmented-Wave Method. *Phys. Rev. B* 1999; 59:1758–75

[26] Perdew JP, Burke K, and Ernzerhof M. Generalized Gradient Approximation Made Simple. *Phys. Rev. Lett.* 1996; 77:3865–8

[27] Bacuyag D, Escaño MCS, David M, *et al.* First-principles study of structural, electronic, and optical properties of surface defects in GaAs(001)-β2(2 × 4). *AIP Adv.* 2018; 8:065012

[28] Bengtsson L. Dipole Correction for Surface Supercell Calculations. *Phys. Rev. B* 1999; 59:12301–4

[29] Monkhorst HJ and Pack JD. Special Points for Brillouin-Zone Integrations. *Phys. Rev. B* 1976; 13:5188–92

[30] Northrup JE and Froyen S. Structure of GaAs(001) Surfaces: The Role of Electrostatic Interactions. *Phys. Rev. B* 1994; 50:2015–8

[31] Hashizume T, Xue QK, Ichimiya A, *et al.* Determination of the surface structures of the GaAs(001)- (2×4) As-rich phase. *Physical Review B* 1995; 51:4200–12

[32] Vlahos V, Booske JH, and Morgan D. Ab initio investigation of barium-scandium-oxygen coatings on tungsten for electron emitting cathodes. *Physical Review B* 2010 Feb; 81(5):054207

[33] Henkelman G, Arnaldsson A, and Jónsson H. A Fast and Robust Algorithm for Bader Decomposition of Charge Density. *Comput. Mater. Sci.* 2006; 36:354–60

https://doi.org/10.66000/3110-9772.2026.02.08

© 2026 Hu *et al.*

This is an open-access article licensed under the terms of the Creative Commons Attribution License (http://creativecommons.org/licenses/by/4.0/), which permits unrestricted use, distribution, and reproduction in any medium, provided the work is properly cited.